ANALYSIS OF AIRFLOW RESISTIVITY AND ACOUSTIC ABSORPTION OF FIBRE-REINFORCED PLASTIC COMPOSITES MADE OF POLYLACTIC ACID AND NATURAL FIBRES

STEHLE, FRANZISKA[1*]; GILLNER, CHRISTIANE[2]; DILBA, BORIS[2]; KEUCHEL, SÖREN[2] AND HERRMANN, AXEL S.[1]

[1] Faserinstitut Bremen e.V., FIBRE, Bremen, Germany
[2] Novicos GmbH, Hamburg-Harburg, Germany

ABSTRACT

This study compares the airflow resistivity and acoustic properties of fibre-reinforced plastic composites (NFRP) with different mixing ratios of polylactic acid (PLA) and the natural fibres flax and cotton for the application in construction as lightweight structures, car door linings or seat pans. The composites are made from the binder fibre PLA, the bast fibre flax and two different kinds of cotton. Nonwovens are consolidated with a thermoforming process to manufacture the NFRP. The addition of cotton improves the absorption by increasing the number of air pockets (pores) and reducing their shape due to the fineness of the cotton. The airflow resistivity of samples with different mixing ratios were analysed and compared. The airflow resistivity is modelled with different calculation models that use distinct material parameters and the transferability is assessed. Further, the absorption coefficient is analysed and compared to the airflow resistivity. The study shows that there is a dependency of the two parameters.

KEYWORDS

Natural fibres; PLA; Fibre-reinforced composites; Thermoforming; Airflow resistivity; Acoustic

INTRODUCTION

Fibre-reinforced plastics made from degradable and renewable raw materials are gaining popularity as sustainable alternatives to materials derived from petrochemicals. Natural fibres contain better hygrothermal properties than petrochemical-based materials [1]. Furthermore, materials derived from petroleum are susceptible to price fluctuations of crude oil, are not renewable, and are predominantly non-biodegradable. On top of that fossil-based products are finite, which creates a need for alternatives [2, 3]. The production of petrochemical materials, as well as their recycling, requires a great deal of energy.

The construction industry is a major consumer of raw materials with 50% of the total consumption, while generating around 60% of the total waste. Only about 10% of the total amount of construction materials needed annually can be recovered [4]. The life-cycle impacts of natural fibres are significantly lower compared to synthetic materials [5]. Acoustic materials made from cellulose and other natural fibres have less embodied energy than polystyrene [6]. The primary energy demand of cellulose fibres is approximately 90% less than of polyurethane rigid foam and 60% less than of rock wool [7].

This highlights the urgent need for a structural shift from petroleum-based products to a bio-based industry. The demand for products made from renewable raw materials is steadily rising in order to create more independence from fossil raw materials.

This study focuses on the development of industrially compostable composites based on renewable resources for the application in architecture as lightweight structures, car door linings or seat pans. The fibres utilized in this research are made of renewable resources: the bioplastic polylactic acid is produced from lactic acid through a fermentation of sugar or starch [8]. The use of renewable raw materials in the form of biopolymers offers the possibility to reduce dependence on petroleum and to use renewable resources instead [9–11]. Another advantage of the bioplastic is the processing on commercially available machinery [12]. Polylactide can be composted in industrial composting plants under the influence of defined moisture and temperature. This produces mainly carbon dioxide

* **Corresponding author:** Stehle F., e-mail: Stehle@Faserinstitut.de
Received November 30, 2023; accepted June 3, 2024

and water, which can be returned to the natural cycle [13]. Cotton and flax as natural fibres are also biodegradable. Thus, the composite can be easily composted on an industrial scale without the need of prior separation. Combining natural fibres and PLA has many advantages such as an improved tensile and flexural strength, elastic modulus and heat distortion [14].

Porous absorbers reduce the sound energy by viscous effects and thermal losses. Throughout the sound absorption, the energy of the sound migrates through the component and viscous effects cause the sound to be dissipated into heat, which is triggered by friction, impulse losses and temperature fluctuations. The developed absorber improves the acoustic by effectively absorbing the sound within the component. Finer fibres improve the viscous losses due to air vibration, since they can shift easier when air vibration occurs [15].

Absorbers partially reflect and absorb sound waves. When sound waves impinge on a surface and are not completely absorbed or reflected, transmission occurs [16]. This principle is shown in the figure 1.

A parameter to classify the acoustic absorbency is the absorption coefficient α. This value is defined by the ratio of the absorbed and the occurred sound energy. When $\boldsymbol{\alpha = 0}$ no sound energy is absorbed, the highest possible number 1 means, that all the energy is absorbed [18].

This active principle is enhanced alongside the thickness and fibre orientation by using an increased fineness of the fibres, which increases the specific surface area, whereby cotton with its unique properties contributes to significant improvements: Compared to other natural fibres cotton is finer, making it an ideal choice for achieving an overall weight reduction in the material [19]. The finer fibres also influence the morphology of the material. The application of fibres with a smaller diameter result in smaller pores since a higher amount of fibres is necessary to form the material with the same weight, but increases the number of the pores and the specific surface area while the volume density remains identical. This results in a higher friction of air molecules [20]. Both physical characteristics improve the sound absorption [21–25]. The reason for this improved absorbency is the possibility of the sound waves entering the material, which reduces the reflection on the surface of the material [15]. The sound waves that enter the material trigger a vibration of the fibres and pores and subsequently an energy conversion into heat [18]. The combination of bast fibres and cotton combines the fibre parameters.

This study describes and investigates the representability of the airflow resistivity of NFRP with models for fibre materials found in the literature. The airflow resistivity can be calculated using parameters such as the fibre diameter and density. Furthermore,

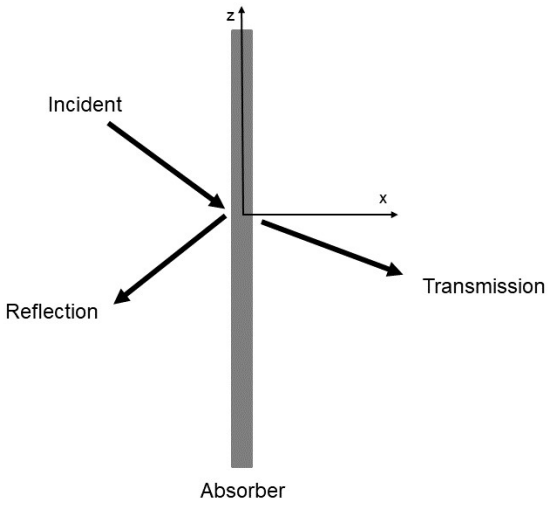

Figure 1. Functional principle of an absorber adapted from [15, 17].

the airflow resistivity and the absorption coefficient of the material are analysed. The relation of these parameters is discussed.

MATERIALS AND METHODS

Manufacturing of the fibre-reinforced composites

Fibres

The fibres utilized in this study consist of the matrix fibre polylactic acid (PLA) as the matrix fibre, along with bast fibres (LI) and cotton (CO). Specifically, the PLA fibres used are the TREVIRA® 400 6.7 dtex shiny rd 60 mm fibres, which possess optimal characteristics for the nonwoven production due to its crimping. The density measures at 1250 kg/m³. Flax fibres were sourced as bast fibres. The fibre diameters were measured with the optical measuring system FibreShape resulting in a mean diameter of 86.16 µm. The length of the fibres ranges from about 10 – 100 mm with a density of 1400 kg/m³ [26]. Additionally, two different types of cotton fibres were employed: long staple fibres from Giza and short staple fibres from Mali. These fibres vary in terms of fineness and length, allowing the evaluation of the distinct influences of each fibre type. The Micronaire which provides information about the maturity and the fibre fineness amounts to 4.14 (Mali) and 4.54 (Giza), the density to 1510 kg/m³ as described in [26]. The diameters, also measured with the FibreShape are on average 12.44 µm (Mali) and 12.30 µm (Giza). The Upper Half Mean Length (UHML) of the short staple fibre was measured at 29.54 mm, while the long staple fibre length was 32.46 mm.

Nonwovens

The nonwovens were manufactured by using a carding machine from TECHNOplants s.r.l. The fibres were opened and blended to ensure a homogenous mixture. Subsequently the carding machine

processed the fibres into webs by individualizing and parallelising the fibres. In the next step the webs were cross-laid and needle punched to form a nonwoven. The resulting nonwoven fabrics had a basis weight of 200 g/m² and a fabric width of 30 cm.

Nonwovens with various mixing ratios were manufactured. Different amounts of matrix fibres (25, 50, 75%) were used as well as assorted amounts of natural fibres. Test specimens without any cotton or bast fibre content were also produced. Short- and long-staple fibre cotton was also applied for the samples. The nonwoven layers, each weighing 200 g/m², were stacked to form a laminate structure prior to the thermoforming process.

Thermoforming

The nonwovens were layered into laminate structures prior to consolidation to increase the total surface weight. Variations of nonwovens with different blending ratios were also implemented. The nonwovens were layered with a 0°/90° layer structure (MD/CD) and then pressed. Different laminate structures were produced. These consisted of four layers of 200 g/m² each with a total basis weight of 800 g/m². The properties of the composites are depicted in Table 1.

The NFRP were produced by consolidating the nonwovens using a two-stage thermoforming process. Two tools were utilised for this purpose: One tool heated by a press melted the fibres under pre-pressure. Subsequently the material was transferred to another tool that consolidated the material by cooling the fibres and thus hardening them. Both tools consisted of a top and bottom plate that are fixed in a press.

The pre-pressure applied to the material by the heated tool was 50 bar. The materials were pressed at 195°C for 10 seconds and then transferred to an unheated press in which the material cooled and the PLA hardens. Thus, the matrix fibre PLA, formed a matrix around the natural fibres, which served as the reinforcing fibres, and solidified the composite, thereby forming a NFRP.

Analysing methods

Scanning electrode microscope (SEM)

The quality of the inner material was examined microscopically in order to be able to optimise the process quality. The degree of melting and the flow behaviour of the melted thermoplastic PLA were determined.

Table 1. Parameters of the composites.

Materials	Mixing ratio				Consolidation parameters		
	PLA	Flax	Cotton (short staple)	Cotton (long staple)	Temperature [°C]	Pressure [bar]	Time [s]
1	25	75	-	-	195	50	10
2	25	37.5	-	37.5			
3	25	-	-	75			
4	50	50	-	-			
5	50	25	25	-			
6	50	25	-	25			
7	50	-	50	-			
8	50	-	-	50			
9	75	25	-	-			
10	75	12.5	-	12.5			
11	75	-	-	25			

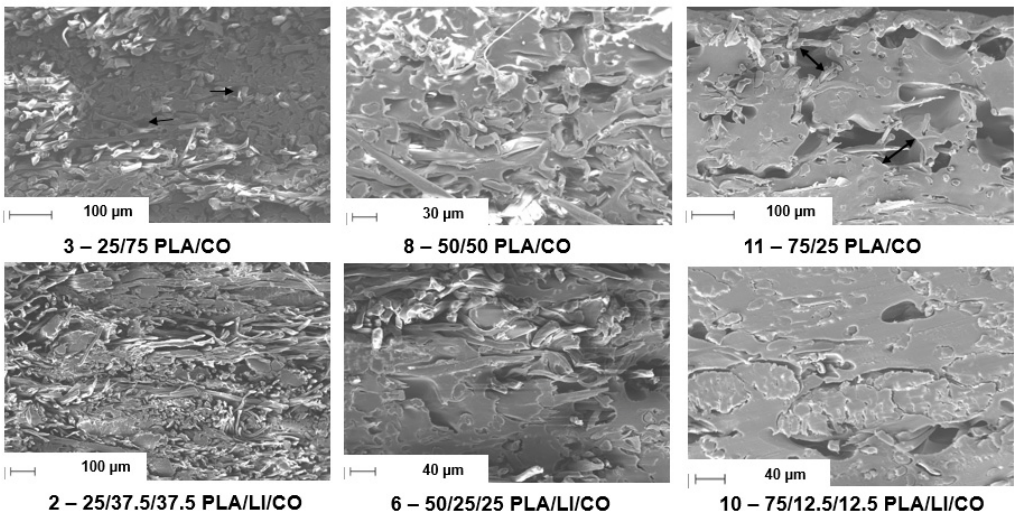

Figure 2. SEM images of the cross-section.

Table 2. Bulk and fibre density of the samples 1-11.

Samples	1	2	3	4	5	6	7	8	9	10	11
ρ_w [kg/m³]	664	591	520	717	732	770	650	745	902	891	875
ρ_f [kg/m³]	1363	1404	1445	1325	1353	1353	1380	1380	1288	1301	1315

Table 3. Calculated porosity of the samples 1-11.

1	2	3	4	5	6	7	8	9	10	11
0.51	0.58	0.64	0.46	0.45	0.52	0.52	0.46	0.35	0.31	0.33

The homogeneity and impregnation of the composite was also tested. Furthermore, the connection of the individual layers of the laminate structure was investigated in order to detect possible air pockets or defects.

Both the cross-section of the materials and the surface were examined.

Figure 2 shows a selection of microscopic images of the cross-section. On the top row the samples 2, 8 and 11 show the different proportion of the PLA combined with cotton fibres, the bottom pictures of the samples 2, 6 and 10 contain cotton fibres as well as flax fibres.

The images show that the PLA fibres are homogeneously fused. No accumulation of matrix can be seen inside the material. The fibres are evenly distributed. The fibres as well as the pores (dark spots) contained in the material are homogeneously distributed in the composite. Due to the layer structure of MD/CD, the directions of the fibres are recognisable, but the connection of the layers appears seamless.

In the cross-section of the material, the SEM images show that the pores are smaller and more frequent in the material with a higher natural fibre content. When the upper left image of sample three is compared to the upper right image of sample 11 with a high amount of PLA, the pores are significantly larger (see marks). This has a positive effect on the acoustic absorption.

The bulk density of the material ρ_w , which is calculated by the mass [kg] and the volume [m³] of the samples is pictured in the following table. The fibre density ρ_f is derived from the density of the fibres according to the amount of fibre in each sample as pictured in Table 1. For example, the fibre density of sample 1 is 1363 kg/m³ since it contains 25% PLA and 75% flax fibres. Samples with 50% cotton and 50% flax fibres as the natural fibre component include the density of flax as well as of cotton in equal parts and the respective amount of PLA. Those values are also listed in Table 2.

The porosity ϕ of the material can be derived from the bulk density of the material $\boldsymbol{\rho_w}$ of the samples and the density of the fibres $\boldsymbol{\rho_f}$ as seen in (1) [27].

$$\boldsymbol{\phi} = \mathbf{1} - \frac{\boldsymbol{\rho_w}}{\boldsymbol{\rho_f}} \quad (1)$$

The results from the calculation for each of the samples are depicted in Table 3.

The porosity of the samples rises with a decreasing quantity of the matrix. The specimen 1-3 with an amount of 25% PLA have the highest porosity compared with their respective samples. The natural fibre content also has an influence on the porosity, as sample with more cotton than flax fibres exhibit a higher porosity. The highest porosity according to the PLA amount is seen in the materials 3, 7, 8 and 11 containing exclusively cotton fibres.

Figure 3 shows the surface of the test specimen 2, 8 and 11 with different amounts of PLA. The matrix and fibre distribution is mostly homogenous, a small collection of PLA is visible on the surface of the sample 11 with a higher PLA content. This can be counteracted by reducing the consolidation time. On the surface of the test specimens, it can be seen clearly that the PLA matrix closes more of the surface with a higher PLA fibre content and therefore reduces the amount of the pores, thus increasing the airflow resistivity. The lower the PLA amount, the more fibres are visible on the surface.

Computed Tomography (CT)

The pores were examined by computed tomography to evaluate the acoustic properties. The CT images were taken with the GE Phoenix V by Baker Hughes system. The measurement time was 20 seconds with 1801 projections.

The sectional image and the volume are shown in Figure 4.

The areas shown in black are hollow spaces in the material. Thus, it is clear that specimen 4 with a mixing ratio of 50/50 PLA/LI has fewer but larger pores than test specimen number 6 with 25% cotton. This observation is also consistent with the analysis of the SEM images. The surface remains open, which preserves the air permeability.

Airflow resistivity

The airflow resistivity was tested according to DIN EN ISO 9053-2:2021-02 Acoustics - Determination of airflow resistance - Part 2: Air exchange flow method [28], with the test device Nor1517A by the Norsonic-

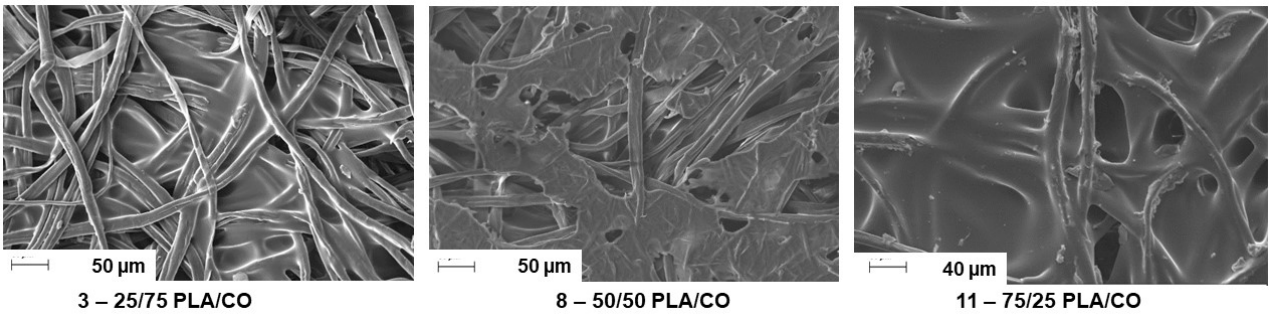

Figure 3. SEM images of the surface of the samples 2, 8 and 11.

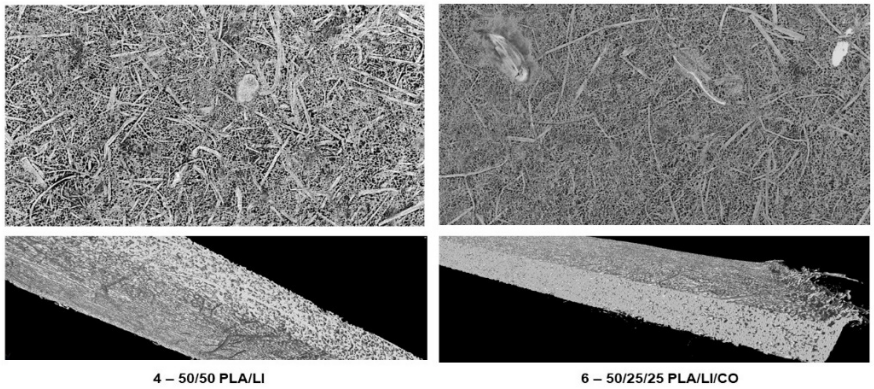

Figure 4. CT images of the sectional view (top) and the volume view (bottom) of the samples 4 and 6.

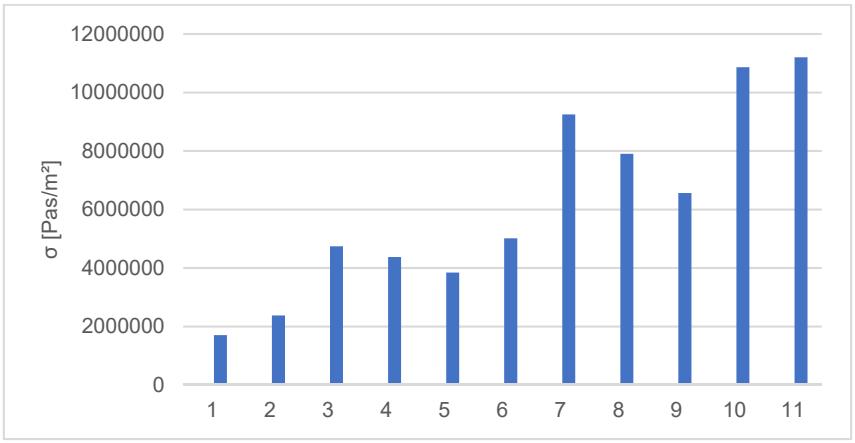

Figure 5. Airflow resistivity of the specimen 1 -11.

Tippkemper GmbH. An air alternating current with a frequency of 2 Hz is generated by means of a pressure vessel and a piston. The alternating current is detected by a microphone. The specific flow resistance R_s [Pas/m] is measured, whereby the airflow resistivity σ [Pas/m²] is calculated by using the thickness d [m] with

$$\sigma = R_s/d \tag{2}$$

The measurements of the specimen are pictured in Figure 5.

The airflow resistivity increases significantly with an increasing proportion of PLA. Test specimens 1-3 with a PLA content of 25% have a lower airflow resistivity according to the relating natural fibre amount than test specimens 4-5 with a 50% PLA content and test specimens 9-11 with a PLA content of 75%. This is due to the fact that the matrix fibre wraps around the natural fibres as a result of melting during the thermoforming process and closes the pores in the material and on the surface. This behaviour is also visible in the SEM images in Figure 2 and Figure 3.

Materials with cotton have a higher airflow resistivity than those with flax fibres. When compared, specimens 1, 4 and 9 with flax fibres and specimens 3, 8 and 11 with cotton, it can be seen that the airflow resistivity is significantly higher. The properties of cotton, such as the fineness of the fibre and the

increased crimping of this fibre, have a positive effect on increasing the airflow resistivity.

Test specimens 5 and 7 with short-staple-fibre cotton and 6 and 8 with long-staple-fibre cotton show that the use of different breeds of cotton results in difference of the airflow resistivity. This is due to the properties of the fibres such as the fibre diameter, the wax content or the maturity.

Acoustic properties

The absorption capacity was examined using an impedance tube according to DIN EN ISO 10534-2 [29]. The absorption coefficient between the frequencies 1000 and 6000 Hz was tested. The sample is clamped in a Kundt's tube without any compression in front of a reverberant wall. White noise in the frequency range mentioned above is excited via a loudspeaker. The acoustic wave is partly reflected by the sample. Two microphones measure the sound pressure, which is a superimposition of the incoming and reflected waves. The absorption coefficient $\boldsymbol{\alpha}$ is calculated by the surface impedance Z_s and the reflection factor r as followed [30]:

$$\boldsymbol{\alpha} = \mathbf{1} - |\boldsymbol{r}|^{\mathbf{2}} \text{ and } r = \frac{1+\widetilde{Z_s}}{1-\widetilde{Z_s}} \quad (3)$$

The acoustic properties were determined based on the absorption coefficient $\boldsymbol{\alpha}$. The Figure 6 pictures the samples 1 – 11.

The absorption coefficient decreases with increasing PLA content, which is due to the surface properties of the specimens with a high matrix content. The higher amount of the thermoplastic matrix reduces the number of pores on the inside and on the surface of the material which increases the reflection of the sound waves. The air pockets inside the samples that diffuse the sound waves are reduced significantly as well. This is seen in samples 2, 6 and 10 with the PLA amounts of 25, 50 and 75% and an even amount of flax and cotton fibres. When comparing the samples 1, 4 and 9 with solely flax fibres as the natural fibre component a similar effect is visible.

The fibres of the samples 9, 10 and 11 that contain 75% PLA are well integrated into the thermoplastic matrix, which leads to a low absorption coefficient, in view of the fact that only a small amount of the sound wave is able to enter into the material and less pores can be found in the material.

Furthermore, the results show, that the material with flax and 25% PLA has a lower absorption compared to the samples which include cotton fibres. The absorption coefficient rises with samples number 2 and 3. The reduced and larger pores of the material with flax due to the larger fibre diameter reduces the sound absorption.

Samples 4, 5, 6, 7 and 8 exhibit a large scattering of the measurements. Nonetheless a rise of the absorption is visible with an increasing amount of cotton fibres.

Concisely materials with a higher amount of cotton fibres exhibit better acoustic properties than those with flax fibres because of the smaller fibre diameter that results in more and smaller pores in the material. The absorption coefficient rises with a decreasing amount of PLA, since the absorber contains more pores inside and on the surface of the material which reduces the reflection.

The relation of the properties can be described as:

$$\alpha_{CO} > \alpha_{CO+LI} > \alpha_{LI} \quad (4)$$

Calculation models of the airflow resistivity

The airflow resistivity σ is an indicator of the acoustic properties of a material. By determining the airflow resistivity, the absorption coefficient α can be modelled to estimate the acoustic absorption. Equally, it is possible to model the airflow resistivity of different materials by incorporating different fibre properties such as the density and fibre diameter. Further parameters needed are the dynamic viscosity of air η (0.82·106 Pas), the massivity μ which can be derived from the following equation [31].

$$\mu = \mathbf{1} - \boldsymbol{\phi} \quad (5)$$

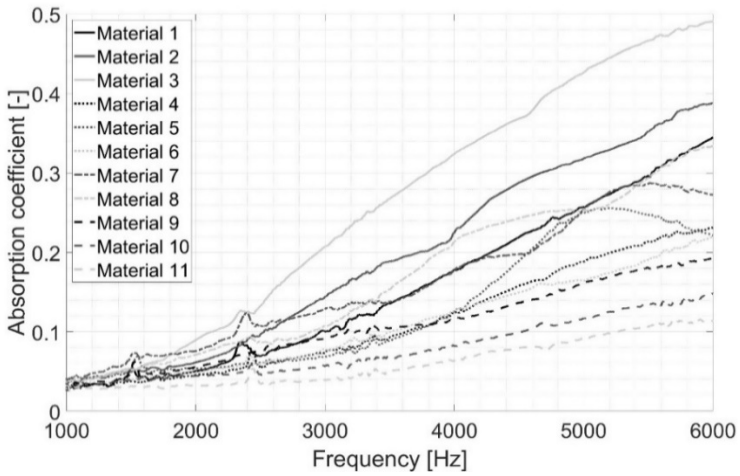

Figure 6. Absorption coefficient of the specimen 1 -11.

There are numerous papers that investigate the correlation of the fibre parameters and the airflow resistivity.

This study presents selected models to calculate the airflow resistivity of fibres and assesses the transferability of these models to NFRPs. The fibre parameters applied for the calculation of the models are listed in chapter 2.1.1.

Various models for calculating the airflow resistivity σ of fibre materials are described in [31] using empirical data from Sullivan. The model (6), here called Mechel Sullivan 1, considers fibre materials for parallel fibre orientation, whereas different fibre radii are being regarded. For this purpose, the parameters fibre radius a [m] as well as the bulk density ρ_w and the density of the fibres ρ_f are used. The airflow resistivity can be calculated from the dynamic viscosity of the air η, the massivity μ determined by the porosity of the material as seen in equation (6).

$$\sigma = \begin{cases} \mathbf{10.56}\frac{\eta}{\boldsymbol{a}^2}\frac{\mu^{\mathbf{1.531}}}{(\mathbf{1}-\mu)^3}; \boldsymbol{a} \approx \mathbf{6-10}\ [\boldsymbol{\mu}\mathbf{m}] \\ \mathbf{6.8}\frac{\eta}{\boldsymbol{a}^2}\frac{\mu^{\mathbf{1.296}}}{(\mathbf{1}-\mu)^3}; \boldsymbol{a} \approx \mathbf{20-30}\ [\boldsymbol{\mu}\mathbf{m}] \end{cases} \quad (6)$$

For the application to the specimens produced in this study, the model for fibre radii of 6-10 µm is used for the cotton content, the flax fibre content is applied to the model with fibre diameters of 20-30 µm. An interpolation is then carried out according to the fibre proportions in order to obtain the result of the "σ" value.

Another model by Mechel Sullivan (7) (Mechel Sullivan 2) considers fibre materials with mono-valued fibre radii and random fibre orientation. This model is also not designed for NFRP. The input parameters are the fibre radius a as well as the density ρ_w and the density of the fibres ρ_f of the material [31].

$$\sigma = 4\frac{\eta}{a^2}\left[0.55\frac{\mu^{4/3}}{(1-\mu)} + \sqrt{2}\frac{\mu^2}{(1-\mu)^3}\right] \quad (7)$$

The Ballagh model [21] is applied to the parameters and compared with the test results. The model is shown under (8). In addition to the density of the material $\boldsymbol{\rho_w}$, Ballagh uses the fibre radius to calculate σ.

$$\sigma = 490{\rho_w}^{1.404}/10^6 a^2 \quad (8)$$

Bies and Hansen [32, 25] work with glass fibres to model the airflow resistivity through porous media by applying the parameters density and the fibre radii. The equation of the model can be seen in (9).

$$\sigma = 27.3\ \mu^{\mathbf{1.53}}(\eta/4a^2) \quad (9)$$

Manning and Panneton present different models for the prediction of the airflow resistivity from the density and fibre diameter D [m] in their work [33]. The model is adjusted to mechanically, resin and thermally bonded fibres. (10) shows the equation for the thermally bonded fibres as this consolidation method is closest to the method applied in this paper.

$$\sigma = \frac{1.94\ 10^{-8}\ \rho_w^{1.516}}{D^2} \quad (10)$$

A model adjusted to multi component polyester fibres is presented in [34]. Yang et al. use three different kind of polyester fibres (regular, hollow and bi-component fibres).

$$\sigma = \frac{1.3395\ 10^{-8}\ \rho_w^{1.565}}{D^2} \quad (11)$$

The approach of a capillary channel theory to predict the airflow resistivity is used by Pelegrinis et al. [35] The porous media is portrayed as a conduit flow between parallel cylindrical capillary tubes. This model adapts the Kozney-Carman model [36] for polyester fibres by an equation (12) that includes fibre diameter and the density of the material, which is used to calculate the massivity as seen in equation and (5).

$$\sigma = \frac{180\ \eta\ \mu^2}{D^2} \quad (12)$$

MODELLING OF THE AIRFLOW RESITIVITY

The calculation models presented in chapter 2.3 were applied to the manufactured test specimens and are shown in the graph below. A comparison was made with the test results of the front and back of the specimen. These are also shown in Figure 7.

The results of the models follow a similar trend compared to the airflow resistivity test results. However, the test results achieve higher results than the modelled values, which shows that the experimental findings cannot be clearly mapped with the models used. This means that there is a need for an adaptation or model for NFRPs.

CONCLUSIONS

NFRP are often made with technical flax. It has been demonstrated that replacing or supplementing the flax fibre material with cotton fibres improves the acoustic absorption of the materials. Increasing the amount of natural fibres as well as the quantity of the cotton fibres has a positive effect as well.

It is evident that the absorption coefficient and the airflow resistivity increase by similar proportions with an increasing cotton content (samples 1-3). The airflow resistivity of the sample 2 is 40% greater than of sample 1, and sample 3 is nearly thrice as high. The absorption coefficient increases at 4000 Hz approx. 40% when comparing samples 1 and 2. Sample 3 is almost twice as high as sample 1. This confirms the correlation of the two parameters. Samples with a high amount of PLA increase the airflow resistivity for the reason that the PLA decreases the permeability of the samples. This effect reduces the absorption coefficient.

The airflow resistivity was mapped with different models based on the density and the fibre radius. The results show that the models for fibre materials, while depicting

a trend, cannot fully represent the airflow resistivity of NFRP.

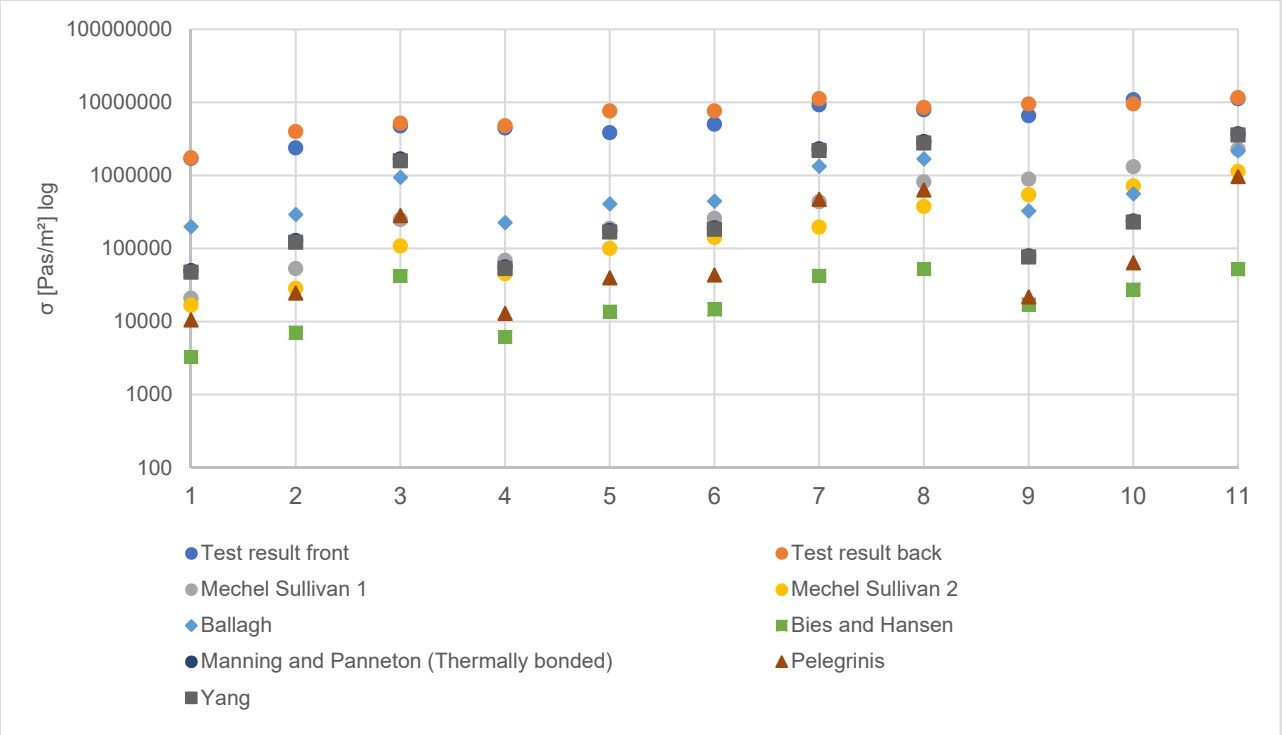

Figure 7. Test results and results of the modelling of the airflow resistivity.

Acknowledgement: *The authors gratefully acknowledge the funding by the Federal Ministry of Food and Agriculture under the grant number 2220NR256A. The responsibility for the content of this publication lies with the authors. The authors declare there is no conflict of interest.*

REFERENCES

1. Berger W., Faulstich H. Fischer P., et al.: Textile Faserstoffe. Springer Berlin Heidelberg, Berlin, Heidelberg, 1993.
2. Hottle T. A., Bilec M. M., Landis A. E.: Sustainability assessments of bio-based polymers. In: Polymer Degradation and Stability, 98(9), 2013, pp. 1898-1907. https://doi.org/10.1016/j.polymdegradstab.2013.06.016
3. Trivedi A. K., Gupta M. K., Singh H.: PLA based biocomposites for sustainable products: A review. In: Advanced Industrial and Engineering Polymer Research, 6(4),2023, pp. 382-395. https://doi.org/10.1016/j.aiepr.2023.02.002
4. Die Zukunft der Bauforschung, 2011, online: https://www.detail.de/artikel/die-zukunft-der-bauforschung-4517/ [cit. 18.09.2023],
5. Ardente F., Beccali M., Cellura M., et al.: Building energy performance: A LCA case study of kenaf-fibres insulation board. In: Energy and Buildings, 40(1), 2008, pp. 1-10. https://doi.org/10.1016/j.enbuild.2006.12.009
6. Asdrubali F.: The role of Life Cycle Assessment (LCA) in the design of sustainable buildings: thermal and sound insulating materials, EURONOISE, 2009, Edinburgh, Scotland.
7. Zabalza Bribián I., Valero Capilla A., Aranda Usón A.: Life cycle assessment of building materials: Comparative analysis of energy and environmental impacts and evaluation of the eco-efficiency improvement potential. In: Building and Environment, 46(5),2011, pp. 1133-1140. https://doi.org/10.1016/j.buildenv.2010.12.002
8. Kayser O., Averesch N.: Technische Biochemie. Springer Fachmedien Wiesbaden, Wiesbaden, 2015.
9. Bauer M., Friede P., Uhlig C.: Sandwiches with Nap Cores. In: Kunststoffe International, 2006, pp. 95-97.
10. Gerber N., Dreyer C., Bauer M.: Noppenwabe als Kernmaterial - Kontinuierlich herstellbares Kernmaterial zur Funktionsintegration in Sandwichbauteilen. In: Konstruktion 3, 2015, pp. 14-16.
11. Ha G. X., Bernaschek A., Zehn M. W.: Experimentally examining the mechanical behaviour of nap-core sandwich material – A novel type of structural composite. In: Journal of Reinforced Plastics and Composites, 38(8), 2019, pp. 369-378. https://doi.org/10.1177/0731684418820437
12. Fachagentur Nachwachsende Rohstoffe e. V. (Hrsg.): Biokunststoffe – Pflanzen, Rohstoffe, Produkte, 2020.
13. Karosseriebautage Hamburg, Proceedings, 2014. http://dx.doi.org/10.1007/978-3-658-05980-4
14. Wu Y., Gao X., Wu J., et al.: Biodegradable Polylactic Acid and Its Composites: Characteristics, Processing, and Sustainable Applications in Sports. In: Polymers, 15(14), 2023. https://doi.org/10.3390/polym15143096
15. Cox T. J., D'Antonio P.: Acoustic absorbers and diffusers – Theory, design, and application. Taylor & Francis, London, 2009.
16. Einführung in die Akustik, 2023, online: https://bauakustik-fachkreis.com/einfuehrung-in-die-akustik/ [cit. 18.09.2023].
17. Möser M.: Technische Akustik. Springer Berlin Heidelberg, Berlin, Heidelberg, 2015.
18. Crocker M. J. (ed.): Handbook of noise and vibration control. John Wiley, Hoboken N. J., 2007.
19. Sciencentris (Hrsg.): Proceedings of the 6th International Conference on Natural Fibers - Nature Inspired Sustainable Solutions, Portugal, 2023.

20. Mamtaz H., Fouladi M. H., Al-Atabi M., et al.: Acoustic Absorption of Natural Fiber Composites. In: Journal of Engineering, 2016. https://doi.org/10.1155/2016/5836107
21. Ballagh K. O.: Acoustical properties of wool. In: Applied Acoustics, 48(2), 1996, pp. 101-120. https://doi.org/10.1016/0003-682X(95)00042-8
22. Ingard K. U.: Notes on sound adsorption technology. Noise Control Foundation, Poughkeepsie, NY, 1995.
23. Hui Z., Fan X.: Sound Absorption Properties of Hemp Fibrous Assembly Absorbers. In: Sen'i Gakkaishi, 65(7), 2009, pp. 191-196. https://doi.org/10.2115/fiber.65.191
24. Samsudin E. M., Ismail L. H., Kadir A. A.: A REVIEW ON PHYSICAL FACTORS INFLUENCING ABSORPTION PERFORMANCE OFFIBROUS SOUN D ABSORPTION MATERIAL FROM NATURAL FIBERS. In: ARPN Journal of Engineering and Applied Sciences, 11(6), 2016.
25. Bies D. A., Hansen C. H., Howard C. Q. (eds.): Engineering noise control. CRC Press, Boca Raton, FL, 2018.
26. Bast and other plant fibres. Textile Institute (Australia), Woodhead Publishing series in textiles no. 39, Woodhead, Cambridge, 2005.
27. ASTM-C0830-00R23: ASTM-C830: Standard Test Methods for Apparent Porosity, Liquid Absorption, Apparent Specific Gravity, and Bulk Density of Refractory Shapes by Vacuum Pressure. Ausgabe August 2023.
28. DIN EN ISO 9053-2:2021-02, Akustik_- Bestimmung des Strömungswiderstandes_- Teil_2: Luftwechselstromverfahren (ISO_9053-2:2020); Deutsche Fassung EN_ISO_9053-2:2020.
29. DIN EN ISO 10534-2:2001-10, Akustik_- Bestimmung des Schallabsorptionsgrades und der Impedanz in Impedanzrohren_- Teil_2: Verfahren mit Übertragungsfunktion (ISO_10534-2:1998); Deutsche Fassung EN_ISO_10534-2:2001.
30. Müller G., Möser M.: Taschenbuch der Technischen Akustik. Springer Berlin Heidelberg, Berlin, Heidelberg, 2016.
31. Mechel F. P. (ed.): Formulas of Acoustics, SpringerLink Bücher, Springer Berlin Heidelberg, Berlin, Heidelberg, 2008.
32. Bies D. A., Hansen C. H.: Flow resistance information for acoustical design. In: Applied Acoustics, 13(5), 1980, pp. 357-391. https://doi.org/10.1016/0003-682X(80)90002-X
33. Manning J., Panneton R.: Acoustical model for Shoddy-based fiber sound absorbers. In: Textile Research Journal, 83(13), 2013, pp. 1356-1370. https://doi.org/10.1177/0040517512470196
34. Yang T., Mishra R., Horoshenkov K. V., et al.: A study of some airflow resistivity models for multi-component polyester fiber assembly. In: Applied Acoustics, 139, 2018, pp. 75-81. https://doi.org/10.1016/j.apacoust.2018.04.023
35. Pelegrinis M. T., Horoshenkov K. V., Burnett A.: An application of Kozeny–Carman flow resistivity model to predict the acoustical properties of polyester fibre. In: Applied Acoustics, 101(5), 2016, pp. 1-4. https://doi.org/10.1016/j.apacoust.2015.07.019
36. DallaValle J. M.: Flow of Gases through Porous Media . P. C. Carman. Academic Press, New York; Butterworths, London, 1956. 182 p. Illus. $6. In: Science 124(3234), 1956, pp. 1254-1255. https://doi.org/10.1126/science.124.3234.1254.b